Inorganic Chemistry

Article

pubs.acs.org/IC

Effects of Hydration during Strontium Exchange into Nanoporous Hydrogen Niobium Titanium Silicate

Samantha Kramer and Aaron J. Celestian*

Geography and Geology, Advanced Materials Institute, Western Kentucky University, 1906 College Heights Boulevard, Bowling Green, Kentucky 42101, United States

Supporting Information

ABSTRACT: A Nb-substituted titanium silicate with the sitinakite (NbTS) topology was exchanged with Sr^{2+} to determine the mechanisms and pathways of ion diffusion through this mixed polyhedral nanoporous framework. The refined structural models yield unit cell parameters and atomic positions of Sr^{2+} and suggest that there was a two-step process during cation diffusion. The starting material of the exchange experiment was the H^+-exchanged material, $H_{1.4}Nb_{0.6}Ti_{1.4}SiO_7 \cdot 1.9H_2O$, with space group $P4_2/mcm$. In the beginning of the exchange process, Sr filled the 8-membered-ring channel near the 4_2 axis in the center. Once the Sr^{2+} fractional occupancy reached approximate 0.11, Sr positions and extra-framework H_2O molecules shifted away from the central 8-membered-ring toward the framework, and an increase in Sr hydration and framework bonding was observed. The new H_2O positions resulted in a lowering of symmetry to the $P\bar{4}2m$ space group, and it is thought that the Sr migration served to enhance Sr^{2+} ion diffusion capacity into the channels of NbTS since the exchange rate briefly accelerated after the 0.11 fractional occupancy level was passed. Exchange of Sr^{2+} into the nanoporous material reached maximum fractional site occupancy of approximately 0.20 using a 10.0 mM $SrCl_2$ solution.

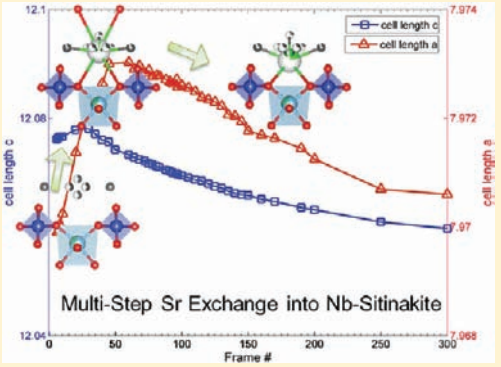

Ion exchange in zeolites and other nanoporous materials has been used for centuries to purify drinking water, in agriculture, and in heavy metal removal from the human digestive system.[1] Only relatively recently have we begun to synthesize enhanced materials with the goal of mimicking sequestration properties of their natural analogues while obtaining higher ion exchange capacities and generating materials for targeted ion selectivity. Ion selective materials have been applied to purification processes in a range of industrial fields and can be used in a variety of matrices (e.g., aqueous solutions, organic solvents, and gases).[2−4]

One important application is the targeted removal of Sr and Cs from nuclear waste disposal sites. Past use of radioactive materials, including government defense activities and nuclear power plants, has produced large quantities of high- and low-level radioactive wastes that require permanent and safe disposal.[5] The radioactive byproducts Sr and Cs from nuclear reactions are generally present in waste solutions at low concentrations (10^{-3}−10^{-5} M),[6] and the waste itself can have a high salinity and typically low pH.[7−9] All materials in contact with byproduct waste solutions should meet several requirements to ensure stability and safety if utilized in the treatment and storage. The sequestration host material must be resistant to radiation as the isotopes ^{90}Sr and ^{137}Cs being γ-emitters with approximate 30 year half-lives.[10] The sequestration material must be highly selective to sequester the targeted species (like Sr and Cs) over the less toxic species like Na or K, and this selective process in nanoporous materials requires their structure to possess unique channel geometries and framework chemistries for targeted ion removal. Also a concern is the thermal stresses, which may induce dehydration of the extra-framework H_2O molecules and hydrolyzation of any remaining metals into metal hydroxides or oxides. Microporous mixed octehadral/tetrahedral silicates (referred to as heterosilicates) have shown to be thermally stable to at least 400 °C,[11,12] ion selective, resistant to high-level waste chemical conditions, and thus a possible candidate material for radioactive waste sequestration.[9]

One nanoporous heterosilicate in particular, naturally occurring as the mineral sitinakite[13] ($HNa_2KTi_4Si_2O_{14} \cdot 4H_2O$), is successful in the selective removal Cs^+ and Sr^{2+} ions from aqueous media.[14−16] Sitinakite (also known as CST or TS in the literature for crystalline silicotitanate or titanium silicate, respectively) can be found in the mines of northern Russia (Kola Peninsula, Khibiny Massif) where it is a secondary mineral phase in hydrothermal systems.[17] TS has only been synthesized with extraframework Na (Na-TS) and ideally crystallizes in a tetragonal space group, $P4_2/mcm$, and unit cell parameters of a = 7.832 Å and c = 11.945 Å.[18] The main structural units are four edge-shared titania octahedra forming cubane-like clusters. These cubane-like clusters form columns of corner-shared titania octahedral groups parallel to [001], and

Received: February 29, 2012
Published: May 23, 2012

the cubane-like groups are connected in the *ab*-plane by silica tetrahedra (Figure 1). The negatively charged framework

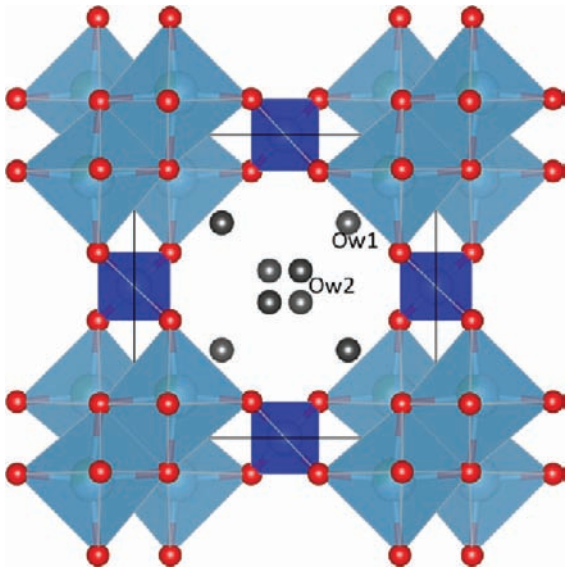

Figure 1. Crystal structure of the H−Nb−sitinakite structure down [001]: Ti (light blue), Si (dark blue), O_{FW} (red), O_{H2O} (black).

encompasses one-dimensional 8-membered-ring (8MR) channels running along the *c*-direction and is neutralized by countercations (e.g,. H^+, Na^+, Cs^+, Sr^{2+}) residing within the 8MR channels. Perpendicular to the 8MR channels are smaller 6MR channels where smaller cations of ionic radii of approximately 1.0 Å (e.g., H^+ and Na^+) are occupied.

The H^+-exchanged sitinakite structure (H-TS, $H_2Ti_2SiO_7{\cdot}1.5H_2O$ $P4_2/mbc$)[19,20] displays more rapid ion diffusion during exchange for the larger alkali ions (e.g., Cs, Sr) compared to Na-TS.[14] Faster ion diffusion has an obvious advantage in potential application of TS materials in nuclear waste remediation. This faster exchange has been explained by the theorized existence of conjugated pπ−dπ orbitals in the O−Ti−O−Si−O bonds,[16] and the double-lever mechanism for the larger Cs ionic radius moves molecular levers which generates a new site for increased exchange capacity and stability.[15] The double-lever mechanism describes a set of cooperative repulsive forces in the channel between the ingoing cation, interstitial H_2O, and framework OH group which initiates conformational changes in the framework and promotes continued ion exchange.

Summarized by Clearfield et al.,[21] H-TS effectively has three exchange sites; one within the framework (center of the 6MR), one near the framework in the 8MR at (z/c = 0, 1/2 in $P4_2/mcm$), and one in the center of the channel of the 8MR (z/c = 1/4, 3/4 in $P4_2/mcm$).[18] When Na^+ is exchanged back into the H-TS structure to a minimum of half occupancy (NaH-$Ti_2SiO_7{\cdot}2H_2O$) in the 6MR the structure reverts back to the initial space group ($P4_2/mcm$). The Na^+ preferentially enters the framework site, within the 6MR, supporting the structure. The Na−O bond distances in the NaH-TS structure were comparable to those in the fully Na^+-exchanged material.[18] Cations of large ionic radius (i.r. > 1 Å) do not fit in the small 6MR and do not force a symmetry change upon ion exchange. Only Cs has been shown to force a conformational change by exchanging into the 8MR channel due to its very large ionic radius.[15,22]

When Sr^{2+} is exchanged into H-TS, Tripathi et al.[23] report several symmetry changes as Sr^{2+} occupancy increases.[24] The disordered arrangement of H_2O molecules and variable coordination environments generate both tetragonal and orthorhombic space groups. Tripathi et al.[24] reported that a 25 mol % exchange of Sr^{2+} into the H-TS structure prompts a conformational change to orthorhombic symmetry (space group *Cmmm*), while the unit cell dimensions remain similar to those of the H^+-exchanged structure. The Sr site has 10-coordination with five framework O^{2-} and five H_2O molecules, and the site resides near the framework at the intersection of the 8MR and 6MR. Further loading to 55 mol % Sr^{2+} converts little more than 80% of the TS back into tetragonal (space group $P4_2/mmc$, a subgroup of the Na-TS group $P4_2/mcm$), and the final powdered sample contains two distinct structures. There are two crystallographic sites for Sr in the $P4_2/mmc$ structure, the first site having 10-coordination (10-CN) to five framework O^{2-} and five H_2O molecules. The other site fills to only half occupancy and has either a 7- or 9-CN, to five framework O^{2-} and the rest supplied by H_2O molecules.[23,24]

In this time-resolved X-ray diffraction study, we substituted some of the Nb for Ti in the framework of sitinakite (NbTS). This substitution reduces the framework negativity compared to TS, which may decrease cation affinity. As with H-TS, H-NbTS possesses fast kinetic properties[14,25,26] and, therefore, is the preferred starting material for ion exchange studies herein.

One distinct advantage of using H-NbTS is that the H^+-exchanged form retains all the symmetry of the synthesized Na-NbTS, space group $P4_2/mcm$. The structure does not collapse, unlike H-TS to $P4_2/mbc$, and the 8MR remain circular. It is assumed that the larger ionic radius of the Nb^{5+} (in 6-CN has an ionic radius of ~0.78 Å while Ti^{4+} in 6-CN is 0.745 Å),[27] and lower H^+ content prevents the structure from twisting into the collapsed geometry. The multistep ion exchange mechanisms of Sr into the H-NbTS are inherently different as compared to H-TS and are a function of both H_2O migration and increased H_2O coordination of Sr as described in this study.

EXPERIMENTAL METHODS

Material Synthesis. Sodium niobium-titanosilicate sitinakite (Na-NbTS), idealized formula of $Na_{1.4}Nb_{0.6}Ti_{1.4}SiO_7{\cdot}H_2O$, has been synthesized by a variety of published processes.[8,18,22,23] One of the more successful procedures for producing crystalline Na-NbTS has been modeled after the work of Poojary et al.[18] and Tripathi et al.[24] The modified synthesis gel was Si:Ti/Nb:Na:H_2O mole ratio of 1:1:10:100, Ti and Nb having a 3:1 ratio (resulting in a 30% Nb substitution as determined from qualitative energy dispersive spectroscopy). The H^+ exchanged structure is prepared by continuously agitating the Na-NbTS in a 1 M hydrochloric acid solution[22] over a period of 48 h.

In Situ Ion Exchange Environmental Cell. The simultaneous collection of diffraction data as Sr^{2+} ions are exchanged into H-NbTS requires the use of the flow-through polyimide environmental cell previously described by Celestian et al. (2008)[15] and is briefly described here. The H-NbTS material is lightly packed into the center of a 5-cm length of polyimide tubing (0.0615-in. inner diameter) and held in place on both sides with glass wool and a 2 cm length spacer with 0.03 in. inner diameter tubing or three 2 cm lengths of 0.01 in. inner diameter tubing. Upchurch unions and flangeless fittings with ferrules attach the polyimide tube to a goniometer head. The environmental cell is connected to the ion solution reservoir via flexible plastic tubing and the exchange solution is advected at low pressure using a peristaltic pump.

dx.doi.org/10.1021/ic300463w | *Inorg. Chem.* 2012, 51, 6251−6258

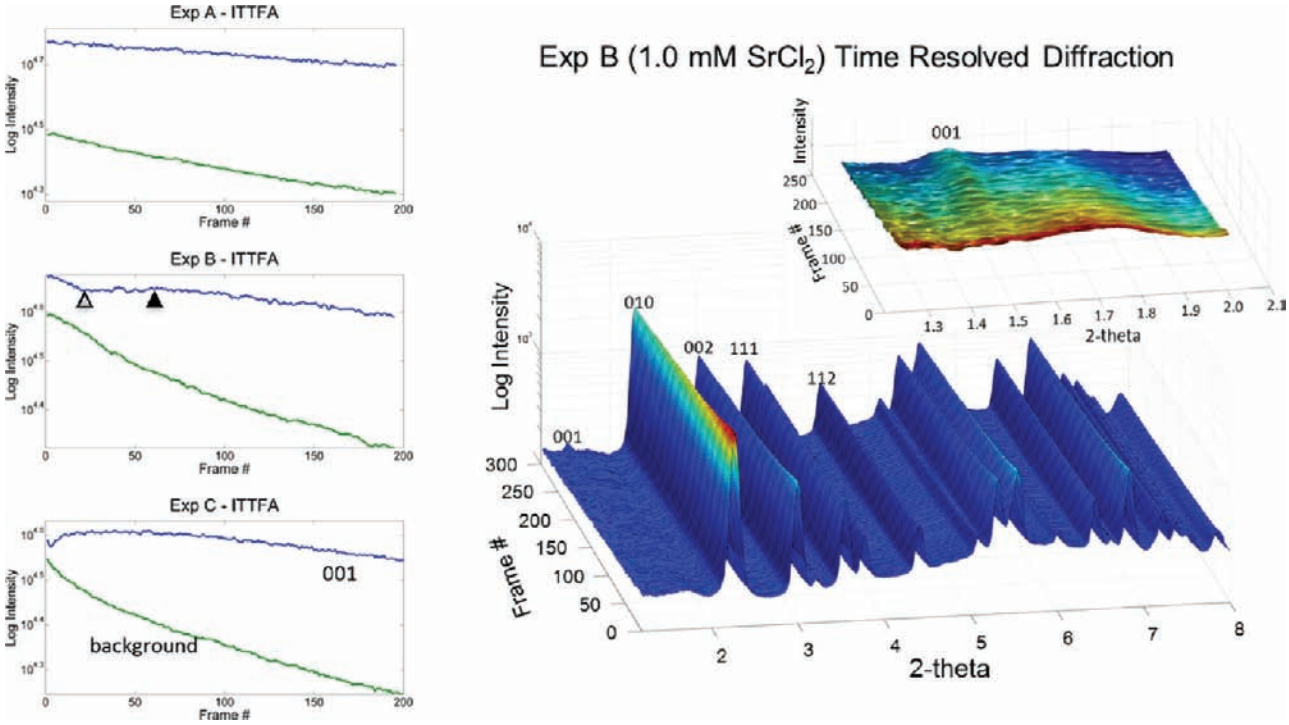

Figure 2. (left) ITTFA plots for each experiment shown as the 001 reflection increases in intensity (blue) above background (green). In exp A, the 001 reflection was not observed and the measured decay parallels the storage ring decay. Exp B ITTFA shows two steps: (1) at frame 20 (open triangle) a leveling of the intensity found in the area of the 001 reflection as background continued to decrease that correlates to the decrease in the *c*-axis cell length and (2) a second decrease step at frame 60 (solid triangle), which correlates to the decrease in the *a*-axis cell length. A similar and more rapid process had also occurred for exp C. (right) Zoomed plot of in situ diffraction data for exp B (1.0 mM $SrCl_2$). (inset) Growth of the weak 001 reflection. Every fifth frame is shown in bold. Time = (frame no.) × (2.5 min).

Three separate ion exchange experiments were conducted in which H-NbTS ($H_{1.4}Nb_{0.6}Ti_{1.4}SiO_7 \cdot 1.9H_2O$) was exchanged with 100 mL of $SrCl_2$ solutions (where exp A = 0.1 mM, exp B = 1.0 mM, and exp C = 10.0 mM $SrCl_2$). The exchange solutions were advected through the sample at a constant rate of approximately 0.5 mL/min in closed circulation. The Sr^{2+} ion solutions were prepared at the Brookhaven National Lab facility by the dissolution of $SrCl_2$ in deionized water provided by the facility.

Powder X-ray Diffraction. A Rigaku Miniflex II X-ray powder diffractometer was used for the ex situ preliminary studies to verify unit-cell parameters of ion exchange materials prior to in situ studies at the National Synchrotron Light Source. On the Rigaku X-ray source, a Cu target ($K\alpha_1 \approx 1.5404$ Å) operating at 20 kV and 5 mA was used to collect data at room temperature between 8° and 65° 2θ, with a step size of 0.02° and a count time of 10 s/step. The diffraction profiles were fit with a Le Bail refinement and unit-cell parameters determined using the Bruker Topas software.

Time resolved in situ diffraction studies were conducted at the National Synchrotron Light Source (NSLS), beamline X7B, Brookhaven National Laboratory, New York. The beamline yields a flux of more than 1×10^{11} photons/s, operating at 38.9 keV, producing X-rays with a wavelength of 0.3184(3) Å. A MAR345 imaging plate detector with a built in scanner is installed on the beamline and was positioned 375 mm from the sample holder during experiments. Scattering data was accumulated in 60-s exposures on the imaging plate, then the plate was scanned, the data exported to the console, and the imaging plate erased. Data could not be collected for approximately 90 s while the imaging plate was scanned and erased. The beam center, detector distance, pitch, and yaw were calibrated with a LaB_6 standard. The goniometer head fitted with the polyimide environmental cell was mounted to the fixed chi circle of the X7B beamline, flexible tubing lines were attached, and the sample was centered in the beam path. Data were collected continuously during each of these experiments, lasting approximately 10 h for each concentration. The imaging plate data were integrated by the software FIT2D[28,29] into an ASCII CHI format (2θ vs intensity). Data could then be converted again with the program ConvX[30] into GSAS (General Structure Analysis Software) and Bruker RAW file format. Iterative targeted transformation factor analyses were performed on the diffraction data to map significant changes in peak intensity and model synchrotron beam decay, while Rietveld structure refinements were completed using Topas, GSAS-EXPGUI,[31,32] and FullProf Suite[33,34] programs.

RESULTS AND DISCUSSION

X-ray Diffraction and Structure Transitions. Several measurable changes were observed in the time-resolved diffraction patterns of all three experiments (Figure 2). The intensity of the low angle 010 reflection quickly decreases upon introduction of the Sr exchange solution. Second, the generation of a new peak is observed in the diffraction pattern at 1.4987° 2θ (d = 12.123 Å) for exp B and exp C, but not observed in exp A (Figure 2).

The new low angle peak in the powder diffraction data was indexed as the 001 reflection by the Crysfire Suite of software,[35] and this reflection is forbidden in the $P4_2/mcm$ space group of H-NbTS. Therefore, the presence of the 001 reflection indicates that a structural transformation occurred. Fitting the diffraction data with the highest signal:noise in the 001 reflection was best done with the last useable diffraction pattern of exp C (10.0 mM Sr^{2+} ion solution). This pattern records the greatest exposure time with Sr, and ideally, the greatest exchange and greatest quantity of structurally transformed material. The most reasonable space group found for the indexed unit cell (SrH-NbTS) was $P\bar{4}2m$, which has a unique set of reflection conditions and is a subgroup (type t, i_t = 2 and i_k = 1)[36−38] of $P4_2/mcm$ (H-NbTS). In comparing the

dx.doi.org/10.1021/ic300463w | Inorg. Chem. 2012, 51, 6251−6258

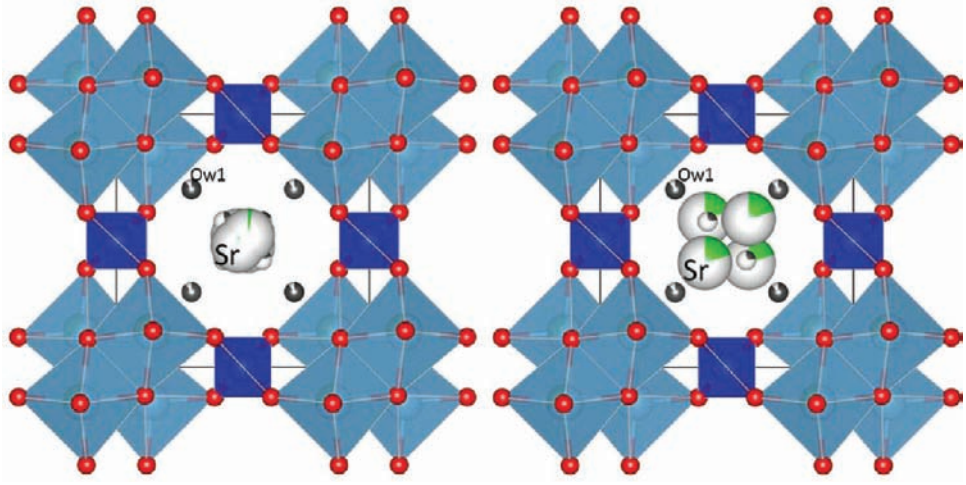

Figure 3. View down [001]. (left) Crystal structure model of Sr sites at the early stages of ion exchange with <0.11 fractional site occupancy. (Right) Sr sites at the final stages of ion exchange with >0.11 fractional site occupancy. After >0.11, Sr fractional site occupancy, the Sr quickly migrates closer to the framework while the new Ow3 site migrates off the Ow2 site, thus changing the symmetry from $P4_2/mcm$ to $P\bar{4}2m$: Ti (light blue), Si (dark blue), O_{FW} (red), O_{H2O} (black), Sr (green).

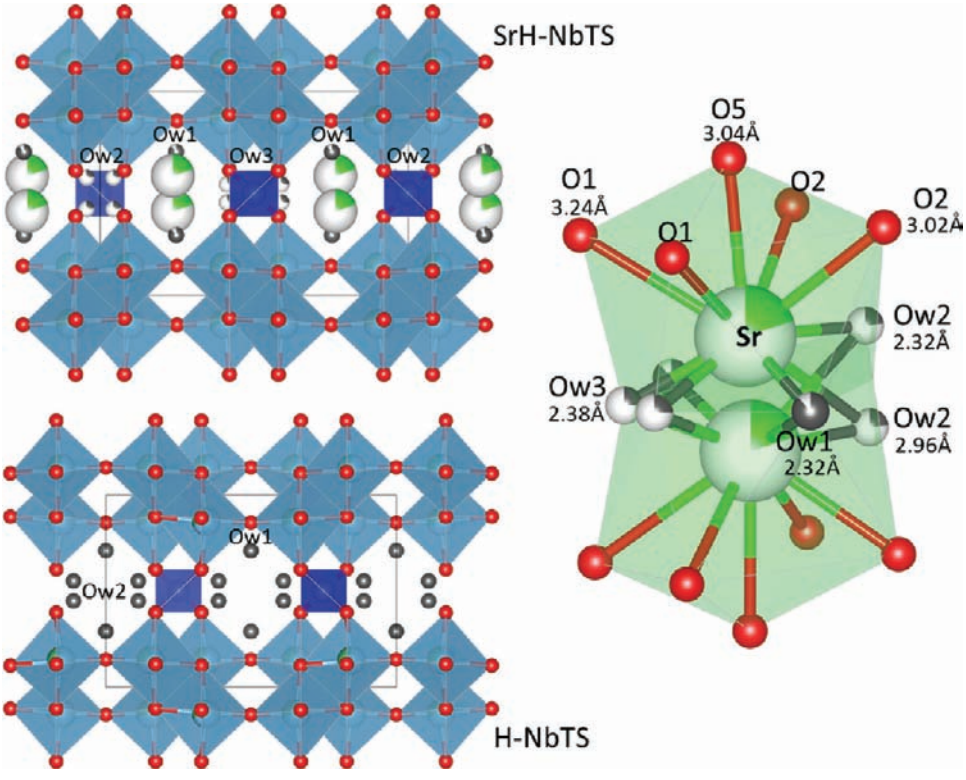

Figure 4. (left) View down [010] showing different O_{H2O} sites. (right) Local Sr site bound to 5 O_{FW} and 6 O_{H2O} sites when Sr fractional site occupancy >0.11. Sites OW1, OW2, and OW3 are labeled in the above figures. The unit cell is outlined in gray. Sr−O bond lengths are indicated under the atom site name.

two symmetries, the Sr-exchanged structure exhibits lower symmetry due to a loss of translation along the *c*-axis, i.e. the 4_2 screw is reduced to a −4, and the transformation matrix is [[1 0 0][0 1 0][0 0 1][0 0 0.25]].

Monitoring the estimated peak evolution of the 001 peak with ITTFA (iterative target transform factor analysis) using in-house software in the Matlab environment statistically confirms the onset times and persistence of the 001 reflection, relative to background, as Sr exchange proceeded in exp B and exp C (Figure 2) In exp A, the 001 reflection did not appear and therefore was not modeled. For Exp B (1.0 mM $SrCl_2$ solution) the 001 reflection can be fit with a fundamental parameters profile function after approximately 150 min (frame 60) from the start of the experiment. In Exp C (10.0 mM $SrCl_2$ solution), the 001 reflection is seen after approximately 16 min (frame 7) and also fit with a fundamental parameters profile function.

Structure Refinements. Structure refinements using the Rietveld method[39] of the first and last in situ diffraction patterns for Exp C indicate that the fractional crystallographic coordinates of the framework metal sites did not move from the

dx.doi.org/10.1021/ic300463w | *Inorg. Chem.* 2012, 51, 6251−6258

Table 1. Results of Selected Refinements and Data Collection Parameters

	frame 10 from exp B	frame 300 from exp B
crystal data[a]	$H_{1.4}Nb_{0.6}Ti_{1.4}SiO_7 \cdot 2H_2O$	$H_{1.04}Sr_{0.18}Nb_{0.6}Ti_{1.4}SiO_7 \cdot 1.3H_2O$
	H-NbTS	SrH-NbTS
	MW_{calc} = 300.84 g/cm^3	MW_{calc} = 303.70 g/cm^3
	tetragonal, $P4_2/mcm$[b]	tetragonal, $P\bar{4}2m$
	a = 7.9703 (4) Å	a = 7.9712 (4) Å
	c = 12.077 (1) Å	c = 12.063 (1) Å
	V = 767.2 (1) Å^3	V = 766.4 (9) Å^3
refinement	Rp = 6.58	Rp = 5.56
	Rwp = 7.38	Rwp = 6.31
	Rexp = 4.20	Rexp = 5.14
	GOF = 1.76	GOF = 1.23
data collection	MAR345 image plate (stationary)	
	T = 25 K	
	λ = 0.3184 Å, Si (111) monochromator, NSLS X7B	
	mount: custom polyimide cell	
	fixed χ =90°	
	2θ fixed = 0°	

[a]All reported measurements are from Rietveld structure refinements. [b]Time resolved data were refined in $P\bar{4}2m$ as explained in the text.

initial H-NbTS structure to the SrH-NbTS ($H_{1.04}Sr_{0.18}Nb_{0.6}Ti_{1.4}SiO_7 \cdot 2H_2O$—as calculated from refined structure and H added for charge balance) structure within 2σ. Therefore the fractional coordinates x, y, z for Ti:Nb and Si sites were fixed for all subsequent refinements as were framework O^{2-} sites. The Ti:Nb occupancy ratio was fixed to 0.70:0.30 and qualitatively verified using energy dispersive spectroscopy, and the results are comparable with previously reported NbTS synthesis.[23,25,40] All examinations of data below 1.2° and above 15.0° 2θ (0.61 Å) were excluded from refinements as data outside these ranges exhibited anomalous integrated intensity variation from being close to the beam stop and detector edges, respectively.

Examination of the experimental data began with the highest concentration and greatest amount of Sr exchange, end of exp C. A new structural model was obtained by transforming the refined $P4_2/mcm$ structure parameters into the $P\bar{4}2m$ space group. Each diffraction pattern examined was first modeled using Le Bail refinements[41] to obtain unit cell parameters (Figure 3) and zero shift errors. The initial diffraction pattern profiles of the wetted H-NbTS powder sample were modeled using a fundamental parameters function as defined in Topas. The background profile was fit using a 12-term shifted Chebyshev function. Single profile manual refinements showed that the difference profile curve could be refined to better than χ^2 = GOF = 2.00 for all diffraction patterns (Figure 4). The results from these Le Bail fits were used in all subsequent Rietveld structure refinements. The unit cell parameters, a and c, were refined for each pattern in the $P\bar{4}2m$ space group starting at frame 1 (Table 1). The $P4_2/mcm$ structure was transformed to the $P\bar{4}2m$ structure for two reasons: (1) there is significant peak overlap between the $P4_2/mcm$ and $P\bar{4}2m$ space groups and it was not possible to distinguish the two during the early stages of ion exchange; (2) modeling the crystal structure and ion exchange processes using a single model rather than a double model approach resulted in the convergence of all least-squares cycles. It is argued later why a single model approach is more useful for this experimental setup. However, the initial structure of H-NbTS was refined in $P4_2/mcm$ for verification of structure and correctness of space group assignment.

Structural models were refined using the Rietveld method[39] to obtain occupancies and positions of the extra framework H_2O molecules (modeled as an O atom and labeled here as O_{H2O} whereas framework O are labeled as O_{FW}) and Sr sites (Figure 5). The framework metal sites and O_{FW} fractional

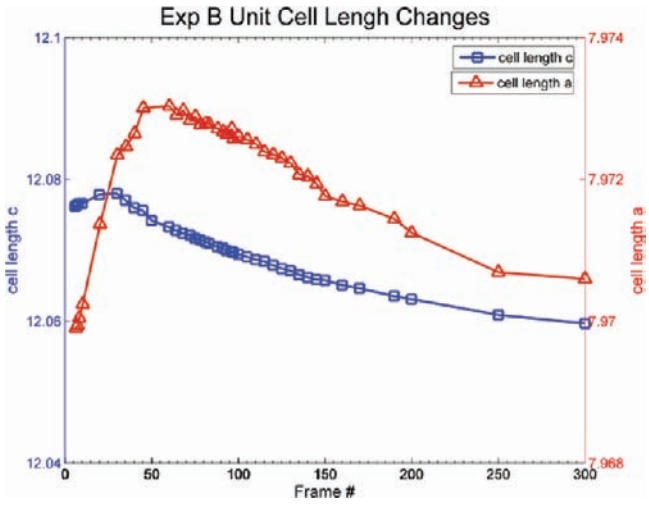

Figure 5. Example plot for unit cell length changes for exp B. The peak in cell length c corresponds to the space group change, and the peak in cell length a corresponds to the Sr site fractional occupancy becoming greater than 0.11 when the Sr migrates to nearer the walls of the 8MR channel. Connecting lines are shown only to guide the eye.

atomic coordinates were not refined for all H-NbTS or SrH-NbTS models because it was determined that the framework positions were identical to >2σ . Fourier difference maps (DELF) were generated from the GSAS/EXPGUI and Topas to visually assess electron density differences between the observed data and the calculated data. This was done by overlying the DELF map outputted by GSAS with the current 3D structure model in VESTA (visualization for electronic and structural analysis program).[42] Peaks found in the DELF maps were placed back into the structure model to better refine positions and occupancies of extra-framework species. This iterative process was continued until residual peak height in the

dx.doi.org/10.1021/ic300463w | Inorg. Chem. 2012, 51, 6251−6258

difference maps were less than 3 eV and that no chemically sensible peaks remained.

Extra-Framework Atomic Positions and Symmetry Change. In refining the final diffraction pattern of exp C, Sr was found to reside near the apical O_{FW} of the Ti/Nb octahedron (O5), bonding to it and the four closest O_{FW} (O1 and O2) sites. This is analogous to the near framework site summarized by Clearfield (2006).[21] Here Sr can attain a total coordination of ten by bonding with five O_{FW} and up to five O_{H2O} molecules (Figures 6 and 7 and Supporting Information Table S1).

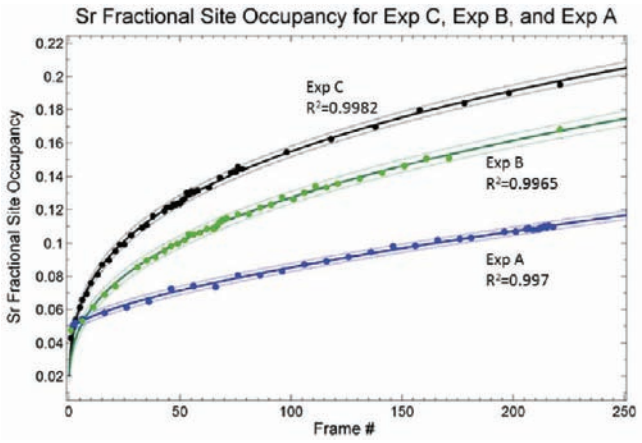

Figure 6. Refined fractional site occupancies for Sr for exp A (blue), exp B (green), and exp C (black). Data are fit with a power function ($f(x) = ax^b + c$), and the 95% confidence level is shown as a faint outline.

Structure refinements with the $P\bar{4}2m$ space group are stable, reaching a convergence GOF value below 2.00 for all data. Attempts to refine the crystal structures using a two-model approach were inconclusive, as there is significant peak overlap and the least-squares refinements could not converge on a minimum. However, it is likely that the transformation from $P4_2/mcm$ to $P\bar{4}2m$ is relatively quick as compared to the speed of data collection and the fast solution flow rate, thus we believe the observed powder diffraction patterns are from the scattering of a single structure type, and not a mixture of $P4_2/mcm$ and $P\bar{4}2m$ in different crystallites. This is currently being verified using 4D (spatial and time-resolved) micro-Raman spectroscopy.

In the maximum Sr-exchanged structure, the H_2O molecules migrate to stabilize the coordination of the larger, more covalent Sr^{2+} ion (compared to H^+ or Na^+). It is this relocation of the O_{H2O} site that forces the loss of symmetry and subsequent space group change from $P4_2/mcm$ to $P\bar{4}2m$, not the position of the Sr site. The space group change only occurred after the Sr fractional occupancy reached ≥0.11 for exp B and C. In exp A, the Sr fractional occupancy did not reach 0.11 (achieving 0.108(4) fractional occupancy), and therefore, no space group change was observed.

The interatomic distances between the Sr and the O_{FW} sites are longer than those to the O_{H2O} sites (Figure 4). The longer Sr−O_{FW} bond is thought to result from the higher O_{FW} coordination with Ti/Nb and the repulsive forces of Ti/Nb, lessening the bond valence of the O_{FW}. The O_{H2O} sites are more closely bound, which supplies the necessary charge balance as indicated by bond valence sum calculations[43] (Supporting Information Table S1).

The O_{H2O} sites labeled as Ow2 in H-NbTS will not occupy the same position within the center of the 8MR in the new $P\bar{4}2m$ unit cell, as it cannot be physically translated along the *c*-axis while Sr fractional site occupancy is <0.11 due to steric constraints. After Sr site occupancy > 0.11, the Ow2 site is split in the new $P\bar{4}2m$ unit cell, labeled as Ow2 and Ow3, and those O_{H2O} sites are partially occupied (Figures 6 and 7). This interstitial H_2O and increasing Sr−Sr interaction likely forces these H_2O molecules closer to the framework causing the loss in symmetry, relieving columbic repulsion between the Sr sites, and thus allowing more Sr^{2+} to enter the structure.

The $P\bar{4}2m$ model derived from the last usable diffraction pattern in exp C was used as the starting model for exp B. The time-resolved compilation of diffraction data by ITTFA showed the presence of the 001 reflection after approximately 150 min (frame 60) of ion exchange (Figure 2). The results from the structure refinements were similar to those in exp C, except the Sr diffusion occurred at a slower rate and did not achieve maximal exchange.

Exp A offered a unique advantaged over exp B and C. The low concentrations used allowed for comparatively slow ion exchange, and the low ionic strength solution did not allow full exchange to occur during the experiment. Here, Sr site occupancy achieved a maximum of 0.108(4) and the measured ITTFA indicates that ion exchange did not force the space group to change. Structural refinements were separately carried out in both space group $P4_2/mcm$ and in $P\bar{4}2m$. Both refinements result in identical structure models, showing Sr nearer to the center of the 8MR channel (at x/a = 0.4801, y/b = 0.4802, and z/c = 0.214 in $P\bar{4}2m$) rather than near the framework (Figures 6 and 7). This experiment suggests that since Sr continues to reside in the center of the 8MR and is not moved closer to the framework, when Sr site occupancy is <0.11, it may be easier to remove Sr from material immersed in solutions of low Sr concentration. Similar effects are seen in equilibrium conditions using amorphous resins (see the work of Helfferich from 1962[44] and references therein).

This Sr-exchanged structure is comparable to the naturally occurring sitinakite. In natural sitinakite, there are two crystallographically distinct K sites and one Na site. The Na site is found within the 6MR and the K sites are found near the center of the 8MR channels (site labeled K2 with 0.079 fractional site occupancy) and at the intersection of the 8MR and 6MR (site labeled K1 with 0.192 fractional site occupancy). We note that the fractional site occupancy dependent sites of Sr in NbTS closely matches the fractional site occupancies of the K1 and K2 sites in sitinakite. In low occupancy stages of Sr-exchange the Sr site closely matches the low occupancy site for K (K2). In higher occupancy stages of Sr exchange, the Sr site closely matches the high occupancy site for K (K1). This correlation between cation occupancy and bonding environment may be a predictive tool for small or divalent cation site selectively during the ion exchange process where the low occupancy sites are filled first, then later in the exchange process, the higher occupancy sites filled.

■ SUMMARY AND CONCLUSIONS

The Sr-exchange mechanisms proposed here are driven by the site positioning of channel species, in that Ow2 requires approximately 0.11 Sr fractional site occupancy before an Ow3 site is created. Prior to the 0.11 occupancy threshold, Sr is

dx.doi.org/10.1021/ic300463w | Inorg. Chem. 2012, 51, 6251−6258

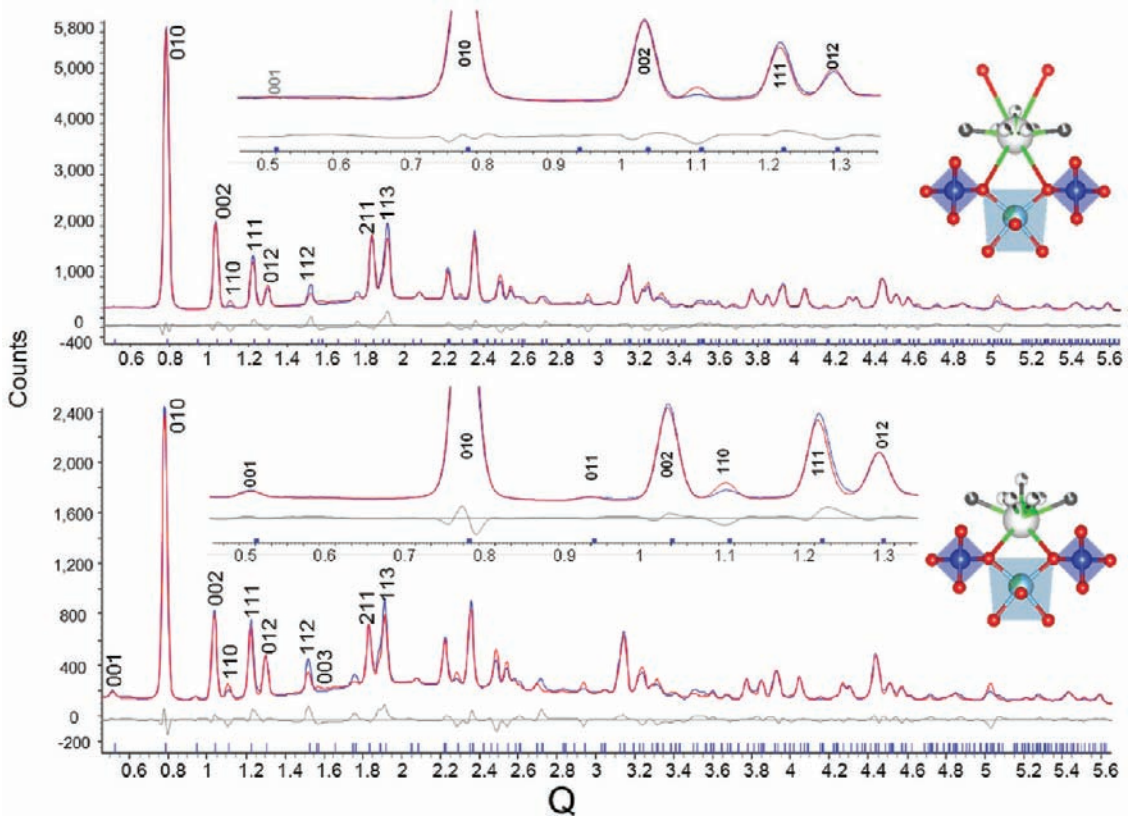

Figure 7. Example Rietveld structure refinement plots for the entire data range in Q for exp B. (top) Frame 10 HSr-NbTS (*Sr* < 0.11) with *a* = 7.9704(4) Å, *c* = 12.077(1) Å. (bottom) Frame 300 SrH-NbTS (*Sr* > 0.11) with *a* = 7.9712(4) Å, *c* = 12.063(1) Å: data (blue), model (red), difference (gray), peak positions (blue ticks). The diffraction inset show the low Q ranges, and structure insets illustrate the Sr−O coordination geometry. New reflections not observed in the $P4_2/mcm$ setting include 001, 012, 003, 021, and 013.

positioned close to the −4 axis in the center of the 8MR channel. After ∼0.11 Sr fractional site occupancy, the preferred bonding orientation is to position Sr near the framework, bonding to five O_{FW}. The remaining bond valence is provided by up to five H_2O molecules and serves to complete the H-bond network to unexchanged H sites. The new Sr position and orientation of the O_{H2O} site within the channel may serve to alleviate space constraints and ionic repulsive forces between the Sr−Sr sites and also increase the hydration coordination of Sr. It is this new O_{H2O} site (Ow3) that is positioned close to the framework and generates a loss in symmetry to the $P\bar{4}2m$ space group. This loss in symmetry was only observed to occur after ∼0.11 Sr fractional site occupancy.

A previous study reported Sr^{2+} exchange Na-NbTS with similar Sr^{2+} ion position in the 8MR channel as our results but being of the $P4_2/mcm$ space group.[24] However, this study has shown that the $P\bar{4}2m$ is likely the correct space group assignment when Sr^{2+} is exchanged into the H-NbTS structure. The observance of the 001 reflection is imperative in modeling the Sr ion diffusion, as the determination the absolute space group would have been ambiguous. Future work using neutron diffraction is planned to carefully model the positional and rotational states of the OH and H_2O groups, which may play critical roles in controlling diffusion rates and symmetry in NbTS. In addition, ongoing work is measuring the reverse exchange properties in the NbTS structure as a function of ion loading concentration. It is hoped this work will assess differences in retention/leaching rates in NbTS as a function of structure and cation coordination.

To date, there are very few time-resolved ion exchanged studies of inorganic materials in the literature, and they have summarized the existence of multiple exchange steps in the diffusion process[15,45] as a function of pore hydration state or interstitial H_2O migration. In addition, there are even fewer ion exchange studies that show conformational changes during cation diffusion where the new crystallographic configurations enhance the diffusion process (e.g. refs 15 and 46−48). The results of this study agree with those previous works stating a multistep exchange mechanism, and possibly the origins of ion selectivity, is strongly influenced by interstitial H_2O or OH dynamics in a wide range of nanoporous systems.

■ ASSOCIATED CONTENT

Ⓢ Supporting Information

CIF files for H-NbTS and SrH-NbTS. This material is available free of charge via the Internet at http://pubs.acs.org.

■ AUTHOR INFORMATION

Corresponding Author

*E-mail: aaron.celestian@wku.edu.

Notes

The authors declare no competing financial interest.

■ ACKNOWLEDGMENTS

We thank the WKU Advanced Materials Institute for support and the National Synchrotron Light Source, Brookhaven National Laboratory, supported by the U.S. Department of

Energy, Office of Science, Office of Basic Energy Sciences, under Contract No. DE-AC02-98CH10886.

REFERENCES

(1) Mumpton, F. A. *Proc. Natl. Acad. Sci.* **1999**, *96*, 3463−3470.
(2) Pang, W.; Yu, J.; Huo, Q. *Chemistry of Zeolites and Related Porous Materials: Synthesis and Structure*; John Wiley & Sons: Sinapore, 2007.
(3) *Natural Zeolites: Occurarence, Properties, Applications*; Bish, D. L., Ming, D. W., Eds.; The Mineralogical Society of America: Washington, D.C., 2001; Vol. *45*.
(4) Harland, C. E. *Ion exchange: theory and practice*; 2nd ed.; Royal Society of Chemistry: Cambridge, 1994.
(5) Ewing, R. C.; Weber, W. J.; Clinard, F. W., Jr. *Prog. Nucl. Energy* **1995**, *29*, 63−127.
(6) Zheng, Z. X.; Gu, D.; Anthony, R. G.; Klavetter, E. *Ind. Eng. Chem. Res.* **1995**, *34*, 2142−2147.
(7) Anthony, R. G.; Dosch, R. G.; Gu, D.; Philip, C. V. *Ind. Eng. Chem. Res.* **1994**, *33*, 2702−2705.
(8) Pertierra, P.; Salvado, M. A.; Garcia-Granda, S.; Bortun, A. I.; Clearfield, A. *Inorg. Chem.* **1999**, *38*, 2563−2566.
(9) Wilmarth, W. R.; Lumetta, G. J.; Johnson, M. E.; Poirier, M. R.; Thompson, M. C.; Suggs, P. C.; Machara, N. P. *Solv. Extr. Ion Exch.* **2011**, *29*, 1−48.
(10) Xu, H. W.; Navrotsky, A.; Nyman, M. D.; Nenoff, T. M. *J. Mater. Res.* **2000**, *15*, 815−823.
(11) Galloway, M. M.; Celestian, A. J.; Parise, J. B.; Clearfield, A.; Perry, H. P. *Abstr. Am. Chem. Soc.* **2006**, *231*, 860-CHED.
(12) Thorogood, G. J.; Kennedy, B. J.; Griffith, C. S.; Elcombe, M. M.; Avdeev, M.; Hanna, J. V.; Thorogood, S. K.; Luca, V. *Chem. Mater.* **2010**, *22*, 4222−4231.
(13) Sokolova, E. V.; Rastsvetaeva, R. K.; Andrianov, V. I.; Egorovtismenko, I. K.; Menshikov, I. P. *Doklady AN SSSR* **1989**, *307*, 114−117.
(14) Celestian, A. J.; Parise, J. B.; Clearfield, A. In *Springer Handbook of Crystal Growth*; Dhanaraj, G., Byrappa, K., Prasad, V., Dudley, M., Eds.; Springer: New York, 2010; pp 1637−1632.
(15) Celestian, A. J.; Kubicki, J. D.; Hanson, J.; Clearfield, A.; Parise, J. B. *J. Am. Chem. Soc.* **2008**, *130*, 11689−11694.
(16) Clearfield, A.; Bortun, L. N.; Bortun, A. I. *React. Funct. Polym.* **2000**, *43*, 85−95.
(17) Menshikov, Y. P.; Sokolova, E. V.; Yegorov-Tismenko, Y. K.; Khomyakov, A. P.; Polezhaeva, L. I. *Zap. Vses. Mineral. Obshch.* **1992**, *121*, 94−99.
(18) Poojary, D. M.; Cahill, R. A.; Clearfield, A. *Chem. Mater.* **1994**, *6*, 2364−2368.
(19) Celestian, A. J.; Parise, J. B.; Smith, R. I.; Toby, B. H.; Clearfield, A. *Inorg. Chem.* **2007**, *46*, 1081−1089.
(20) Clearfield, A. *Solid State Sci.* **2001**, *3*, 103−112.
(21) Clearfield, A.; Tripathi, A.; Medvedev, D.; Celestian, A. J.; Parise, J. B. *J. Mater. Sci.* **2006**, *41*, 1325−1333.
(22) Poojary, D. M.; Bortun, A. I.; Bortun, L. N.; Clearfield, A. *Inorg. Chem.* **1996**, *35*, 6131−6139.
(23) Tripathi, A.; Medvedev, D. G.; Clearfield, A. *J. Solid State Chem.* **2005**, *178*, 253−261.
(24) Tripathi, A.; Medvedev, D. G.; Nyman, M.; Clearfield, A. *J. Solid State Chem.* **2003**, *175*, 72−83.
(25) Chitra, S.; Viswanathan, S.; Rao, S. V. S.; Sinha, P. K. *J. Radioanal. Nucl. Chem.* **2011**, *287*, 955−960.
(26) Milne, N. A.; Griffith, C. S.; Hanna, J. V.; Skyllas-Kazacos, M.; Luca, V. *Chem. Mater.* **2006**, *18*, 3192−3202.
(27) Shannon, R. D.; Prewitt, C. T. *Acta Crystallogr., Sect. B* **1970**, *B 26*, 1046.
(28) Hammersley, A. P. *FIT2D: V9.129 Reference Manual V3.1*, ESRF, 1998.
(29) Hammersley, A. P.; Svensson, S. O.; Hanfland, M.; Finch, A. N.; Hausermann, D. *High Pressure Res.* **1996**, *14*, 235−248.
(30) Bowden, M. *ConvX*, Conversion Program for X-ray Diffraction Data; 1998. (http://www.ccp14.ac.uk/ccp/web-mirrors/convx/), accessed on May 21, 2012.
(31) Toby, B. H. *J. Appl. Crystallogr.* **2001**, *34*, 210−213.
(32) Larson, A. C.; VonDreele, R. B. *General Structure Analysis System (GSAS)*, Los Alamos National Laboratory Report LAUR 86-748; 2000.
(33) Gonzalez-Platas, J.; Rodriquez-Carvajal, J. *"Recent Developments of the Program FULLPROF"* in Commission on Powder Diffraction IUCr Newsletter; 2001, *26*, 12−19.
(34) Roisnel, T.; Rodriguez-Carvajal, J. *Mater. Sci. Forum* **2001**, *378−3*, 118−123.
(35) Shirley, R. *Acta Cryst.* **2000**, *A56* (Supplement), s350.
(36) Aroyo, M. I.; Kirov, A.; Capillas, C.; Perez-Mato, J. M.; Wondratschek, H. *Acta Crystallogr., Sect. A* **2006**, *62*, 115−128.
(37) Aroyo, M. I.; Perez-Mato, J. M.; Capillas, C.; Kroumova, E.; Ivantchev, S.; Madariaga, G.; Kirov, A.; Wondratschek, H. *Z. Kristallogr.* **2006**, *221*, 15−27.
(38) Aroyo, M. I.; Perez-Mato, J. M.; Orobengoa, D.; Tasci, E.; de la Flor, G.; Kirov, A. *Bulgarian Chem. Commun.* **2011**, *43*, 183−197.
(39) Rietveld, H. M. *J. Appl. Crystallogr.* **1969**, *2*, 65−71.
(40) Luca, V.; Hanna, J. V.; Smith, M. E.; James, M.; Mitchell, D. R. G.; Bartlett, J. R. *Micropor. Mesopor. Mat.* **2002**, *55*, 1−13.
(41) Le Bail, A.; Duroy, H.; Fourquet, J. L. *Mater. Res. Bull.* **1998**, *23*, 447−452.
(42) Momma, K.; Izumi, F. *J. Appl. Crystallogr.* **2011**, *44*, 1272−1276.
(43) Wills, A. S. *VaList*, 2011; program available from www.ccp14.ac.uk.
(44) Helfferich, F. *Ion Exchange*; McGraw-Hill Book Company, Inc.: New York, 1962.
(45) Lopano, C. L.; Heaney, P. J.; Post, J. E. *Am. Mineral.* **2009**, *94*, 816−826.
(46) Celestian, A. J.; Parise, J. B.; Goodell, C.; Tripathi, A.; Hanson, J. *Chem. Mater.* **2004**, *16*, 2244−2254.
(47) Ding, N.; Kanatzidis, M. G. *Nat. Chem.* **2010**, *2*, 187−191.
(48) Doyle, D. A.; Cabral, J. M.; Pfuetzner, R. A.; Kuo, A. L.; Gulbis, J. M.; Cohen, S. L.; Chait, B. T.; MacKinnon, R. *Science* **1998**, *280*, 69−77.